Loss of the deubiquitinase USP36 destabilizes the RNA helicase DHX33 and causes preimplantation lethality in mice

Julia M. Fraile[‡], Diana Campos-Iglesias[‡], Francisco Rodríguez[‡], Aurora Astudillo[§], Roser Vilarrasa-Blasi[¶], Nuria Verdaguer-Dot[¶], Miguel A. Prado[‖], Joao A. Paulo[‖], Steven P. Gygi[‖], José I. Martín-Subero[¶],
[ORCID] José M. P. Freije[‡**1], and Carlos López-Otín[‡**2]

From the [‡]Departamento de Bioquímica y Biología Molecular, Facultad de Medicina, Instituto Universitario de Oncología (IUOPA), Universidad de Oviedo, 33006-Oviedo, Spain, the [§]Servicio de Anatomía Patológica, Hospital Universitario Central de Asturias, 33006-Oviedo, Spain, the [¶]Departamento de Anatomía Patológica, Farmacología y Microbiología, Universitat de Barcelona, IDIBAPS, 08036-Barcelona, Spain, the [‖]Department of Cell Biology, Harvard Medical School, Boston, Massachusetts 02115, and the [**]Centro de Investigación Biomédica en Red de Cáncer, Spain

Edited by Eric R. Fearon

Deubiquitinases are proteases with a wide functional diversity that profoundly impact multiple biological processes. Among them, the ubiquitin-specific protease 36 (USP36) has been implicated in the regulation of nucleolar activity. However, its functional relevance *in vivo* has not yet been fully described. Here, we report the generation of an Usp36-deficient mouse model to examine the function of this enzyme. We show that Usp36 depletion is lethal in preimplantation mouse embryos, where it blocks the transition from morula to blastocyst during embryonic development. USP36 reduces the ubiquitination levels and increases the stability of the DEAH-box RNA helicase DHX33, which is critically involved in ribosomal RNA synthesis and mRNA translation. In agreement with this finding, *O*-propargyl-puromycin incorporation experiments, Northern blot, and electron microscopy analyses demonstrated the role of USP36 in ribosomal RNA and protein synthesis. Finally, we show that *USP36* down-regulation alters cell proliferation in human cancer cells by inducing both apoptosis and cell cycle arrest, and that reducing DHX33 levels through short hairpin RNA interference has the same effect. Collectively, these results support that Usp36 is essential for cell and organism viability because of its role in ribosomal RNA processing and protein synthesis, which is mediated, at least in part, by regulating DHX33 stability.

Deubiquitinases, or DUBs,[3] are a large group of proteases with the ability to hydrolyze the isopeptide bond that link ubiq-uitin chains to target proteins (1–4). There are six families of DUBs grouped according to sequence and structural similarities: ubiquitin-specific proteases (USPs), ubiquitin carboxyl-terminal hydrolases, ovarian-tumor proteases, Machado-Joseph disease protein domain proteases (MJDs), JAMM/MPN domain-associated metallopeptidases (JAMMs), and monocyte chemotactic protein-induced protein family (5). Over the last years, DUBs have attracted especial interest due to their wide functional diversity and profound impact on the regulation of multiple biological processes (2, 6, 7). The cysteine proteases of the USP family represent the largest group of DUBs, with more than 50 members in humans (8–10). Among them, USP36 has been related to nucleolar activity regulation, through the deubiquitination of nucleophosmin/B23 and fibrillarin (11, 12). Additionally, USP36 activity has also been implicated in autophagy activation (13), as well as in oxidative stress regulation by the stabilization of mitochondrial superoxide dismutase SOD2 (14). Interestingly, the *Drosophila* gene *scrawny* (*scny*), which encodes an USP family protein homologous to human USP36, has been described to inhibit H2B ubiquitination, repressing the premature expression in stem cells of key differentiation genes (15). The role of USP36 in the stabilization of the oncogene c-Myc has also been reported (16). Finally, it has been proposed that USP36 is critical for ribosome biogenesis through the regulation of RNA polymerase I stability (17, 18).

Over the last years, several studies have shown that RNA helicases comprise the largest family of enzymes that regulate RNA metabolic processes, such as pre-mRNA splicing, RNA editing, mRNA translation, and ribosome biogenesis (19). In fact, it has been widely described that most RNA helicases contribute to several steps of RNA metabolism, coordinating and orchestrating gene expression patterns. The human genome encodes 15 DEAH-box RNA helicases, which are RNA-binding proteins with the ability to modify RNA structure through the hydrolysis of ATP. One of these family members, DHX33, has been implicated in nucleolar organization, ribosome biogene-

[3] The abbreviations used are: DUB, deubiquitinase; USP, ubiquitin-specific protease; dpc, days postcoitum; TMT, tandem mass tag; P-LISA, Duolink *in situ* proximity ligation assay; shRNA, short hairpin RNA; PI, propidium iodide; TUNEL, deoxynucleotidyltransferase-mediated dUTP nick end labeling; FA, formic acid; ACN, acetonitrile; AGC, automatic gain control; HA, hemagglutinin; EGFP, enhanced green fluorescent protein; IP, immunoprecipitation; MEF, mouse embryonic fibroblast; OP-Puro, *O*-propargyl-puromycin; PARP, poly(ADP-ribose) polymerase; MTT, 3-(4,5-dimethylthiazol-2-yl)-2,5-diphenyltetrazolium bromide.
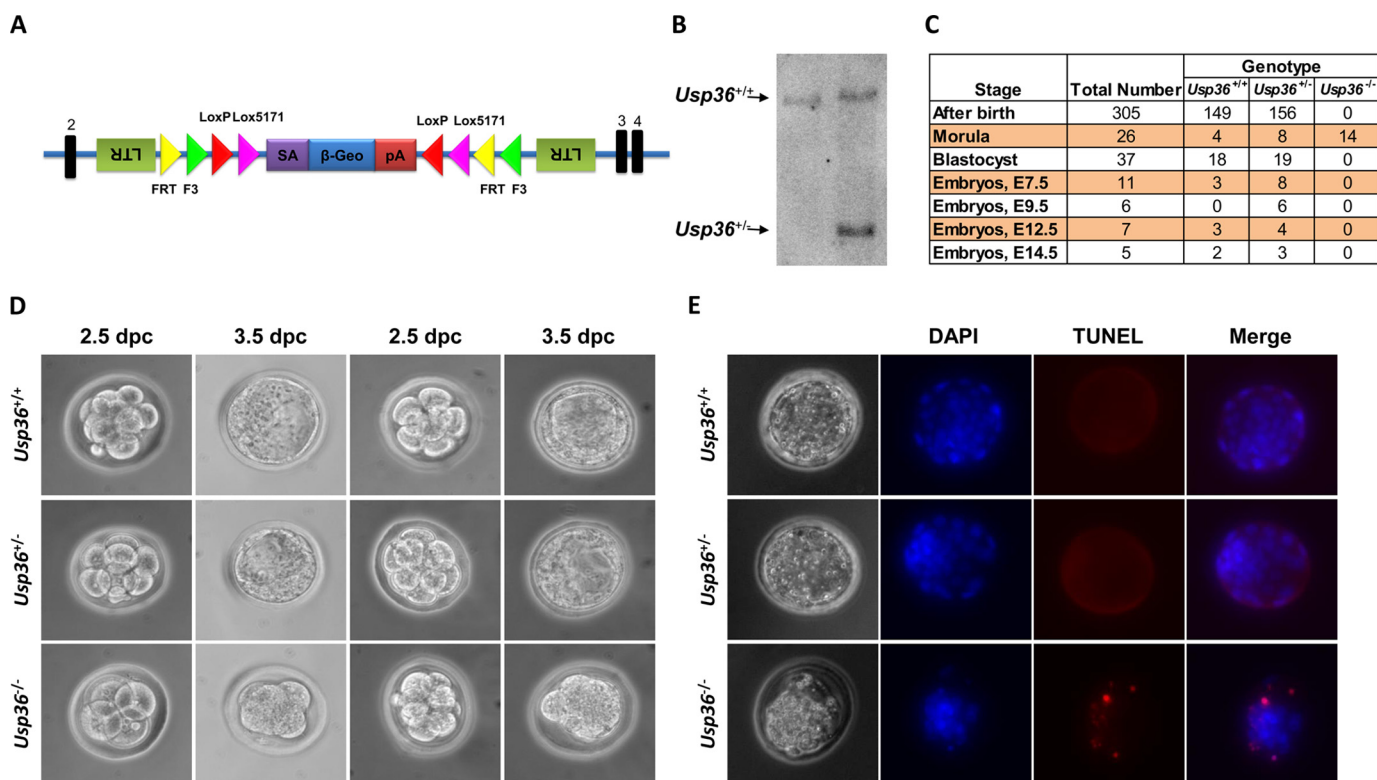
Figure 1. Usp36 depletion leads to preimplantation lethality. *A,* schematic representation of the gene trap strategy used for the generation of the *Usp36*-deficient mouse model. *B,* Southern blot analysis performed on wildtype and *Usp36*-heterozygous mice. *C,* distribution of genotyped offspring and embryos from *Usp36*^+/− intercrosses. *Usp36*^−/− embryos were not found beyond the morula stage. *D,* representative images of embryos obtained from heterozygous intercrosses of *Usp36*^+/− mice obtained at 2.5 dpc (morulae) and cultured *in vitro* for 24 h (blastocysts, 3.5 dpc). *E,* TUNEL staining of 3.5 dpc embryos revealed apoptosis in *Usp36*-depleted morulae.

sis, and protein synthesis. Thus, DHX33 promotes mRNA translation initiation by regulating elongation-competent 80S ribosome assembly (20) and modulates RNA polymerase I–directed transcriptional activity through its interaction with the DNA chromatin-modulating protein UBF (21).

In this work, the generation and characterization of mutant mice deficient in Usp36 revealed that this DUB is an essential enzyme for embryonic development. Additionally, this study provides evidence that Usp36 regulates ribosomal RNA and protein synthesis, and proposes a regulatory function for this protease on the ubiquitination status and stability of Dhx33. Altogether, these data identify USP36 as a deubiquitinating enzyme whose function in rRNA processing and mRNA translation is critical for cell and organism viability.

Results

Usp36 deletion leads to embryonic lethality in mice

To study the biological function of the deubiquitinase USP36, the *Usp36* gene was disrupted in mice by homologous recombination using a gene trap strategy (Fig. 1*A*). Heterozygosity for the mutation was confirmed by Southern blot analysis (Fig. 1*B*). *Usp36* heterozygous mice were fertile and healthy with no obvious abnormalities. However, when these mice were intercrossed, no homozygous pups were detected at weaning (Fig. 1*C*), suggesting that the complete absence of Usp36 causes embryonic lethality. To further analyze how Usp36 deficiency affects embryogenesis, embryos were collected at different stages of development, from 2.5 to 14.5 days postcoitum (dpc).

As shown in Fig. 1*C*, homozygous mice were detected only at the morula stage. To characterize the role played by Usp36 during the critical transition from morula to blastocyst, embryos at 2.5 dpc were extracted and cultured *in vitro*. The next day, some of them had developed into blastocysts, whereas other remained at the morula stage. A high proportion of these morulae carried the homozygous mutation (Fig. 1*D*), whereas, by contrast, all the blastocysts were wildtype or heterozygous for *Usp36*.

To elucidate the mechanism by which *Usp36*^−/− blastocysts are unviable, TUNEL analysis was performed in these embryos. Only 1 of 4 wildtype and 2 of 5 heterozygous morulae were positive for TUNEL staining, whereas 4 of 4 *Usp36*-deficient arrested morulae showed apoptotic markers, suggesting that Usp36 deficiency activates apoptotic pathways that could impede the transition from morula to blastocyst. Taken together, these results demonstrate that Usp36 is essential for embryo development and that its deficiency induces an apoptotic response at the morula stage that leads to preimplantation lethality.

USP36 regulates DHX33 ubiquitination levels

To investigate the biochemical function of USP36, characterization of the proteomic profile of wildtype and Usp36-deficient cells was undertaken. With this purpose, quantitative mass spectrometry analysis using a tandem mass tag (TMT) technique was performed with protein extracts from wildtype and *Usp36*-heterozygous MEFs by triplicate. This proteomic
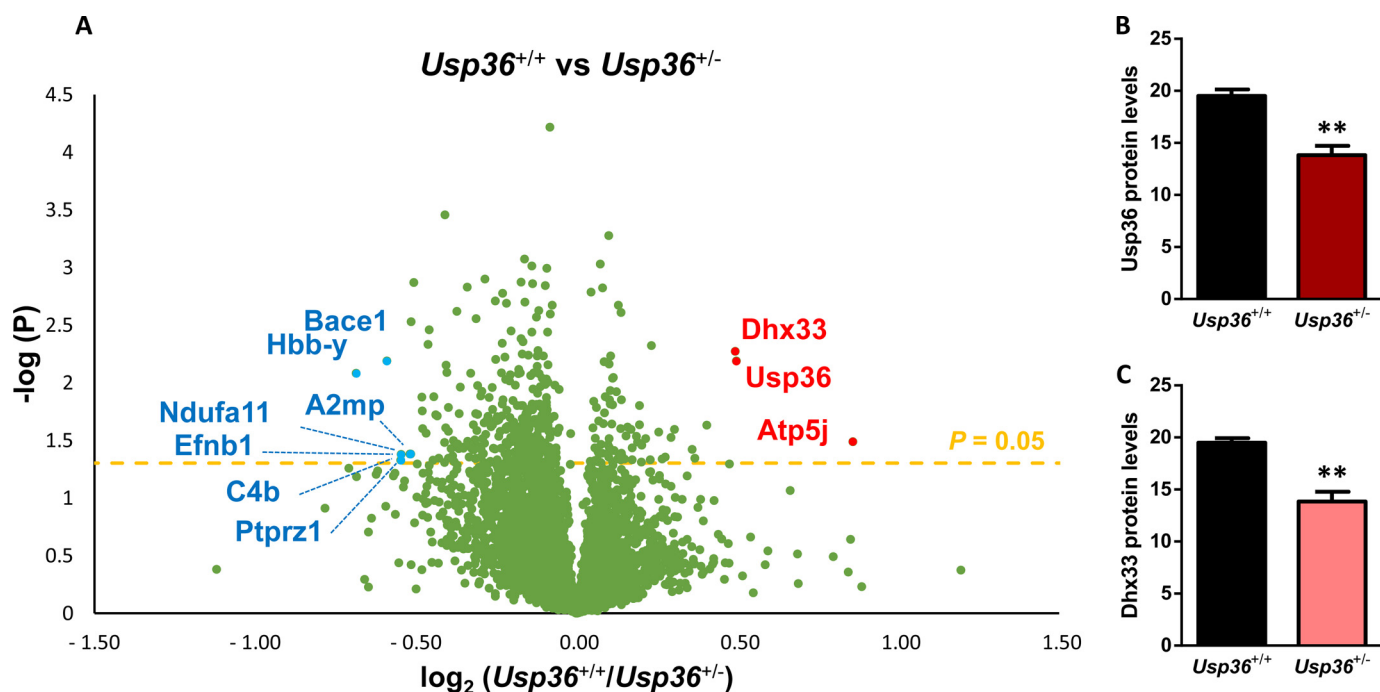
Figure 2. Dhx33 protein levels are reduced in *Usp36*-heterozygous MEFs. *A*, volcano plot showing the results obtained from protein extracts of *Usp36*^+/+^ and *Usp36*^+/−^ MEFs that were analyzed by mass spectrometry using TMT technique. Data are represented as the ratio *Usp36*^+/+^ *versus Usp36*^+/−^, which was calculated as the mean of the normalized signal obtained in *Usp36*^+/+^ MEFs divided by the mean of the normalized signal obtained in *Usp36*^+/−^ MEFs ($n = 3$ biological replicates). *B* and *C,* Usp36 and Dhx33 protein levels from wildtype and *Usp36*-heterozygous MEFs, assessed by mass spectrometry, two-tailed Student's *t* test (**, $p < 0.01$).

approach allowed us to quantify over 7,200 proteins, revealing changes in 251 proteins (Fig. 2*A* and Table S1). This analysis showed that Usp36 protein levels in *Usp36*^+/−^ MEFs were about 70% of those in *Usp36*^+/+^ fibroblasts (Fig. 2*B* and Table S1). Similarly, the levels of Dhx33, a pivotal DEAH-box RNA helicase involved in RNA polymerase I-mediated transcription (21), were also reduced in *Usp36*^+/−^ MEFs to 70% of control samples (Fig. 2*C* and Table S1). Dhx33 down-regulation in MEFs was validated by Western blot (Fig. 3*A*). Next, *Usp36*^+/+^ and *Usp36*^+/−^ MEFs were treated with 1 μM bortezomib during 18 h. As shown in Fig. 3*A*, proteasome inhibition induced the accumulation of Dhx33 in *Usp36*^+/−^ MEFs, to the same extent as in wildtype MEFs, supporting that Dhx33 is regulated by the ubiquitin-proteasome system. To investigate if USP36 and DHX33 proteins interact each other, the human *USP36* cDNA was cloned fused to the C-terminal of GFP and overexpressed into HEK-293T cells, together with pLVX–FLAG–DHX33. Co-immunoprecipitation assays confirmed that ectopically expressed GFP–USP36 could be detected in FLAG-tagged DHX33 immunoprecipitates (Fig. 3*B*). In agreement with these results, colocalization of USP36 and DHX33 was observed through immunofluorescence analysis in HeLa cells transfected with pLVX–FLAG–DHX33 and GFP–USP36 (Fig. 3*C*). Furthermore, a Duolink In Situ Proximity Ligation Assay (P-LISA) (22) showed that GFP-USP36 directly interacted with FLAG-tagged DHX33 protein (Fig. 3*D*), supporting the interaction between both proteins. These findings are consistent with the results from reported global proteomic studies (23, 24) (Fig. S1) and a yeast two-hybrid assay (25), which confirms the interaction between USP36 and DHX33.

To investigate whether USP36 regulates DHX33 levels through deubiquitination, HEK-293T cells were transfected with HA–ubiquitin and pLVX–FLAG–DHX33, with or without *USP36* overexpression. After treatment with bortezomib, DHX33 was immunoprecipitated and its ubiquitination status was analyzed using both anti-HA and anti-DHX33 antibodies. As shown in Fig. 3*E*, USP36 overexpression reduced DHX33 ubiquitination and, accordingly, led to increased levels of ectopically expressed DHX33. On the contrary, HEK-293T transfected with an *USP36*-specific shRNA showed an increase in DHX33 ubiquitination levels (Fig. 3*F*). Altogether, these results support that USP36 stabilizes DHX33 through the regulation of its ubiquitination status.

Usp36 deficiency impairs mRNA translation and rRNA synthesis

The essentiality of Usp36 at an early stage of development demonstrates its involvement in critical biological functions. Among the molecular changes occurring at the transition from morula to blastocyst, rDNA transcription and nucleoli maturation have been reported to occur beyond the morula stage. In this regard, DHX33 has a pivotal role as a promoter of mRNA translation initiation (20). These facts suggested that USP36 deubiquitinase activity could have a role in protein synthesis, at least in part, through the stabilization of DHX33. To investigate *in vivo* the role of Usp36 in this physiological process, morulae at 2.5 dpc from intercrosses between *Usp36*-heterozygous mice were extracted. At 3.5 dpc, embryos were treated with *O*-propargyl-puromycin (OP-Puro), an alkyne analog of puromycin that forms covalent conjugates with nascent polypeptide chains
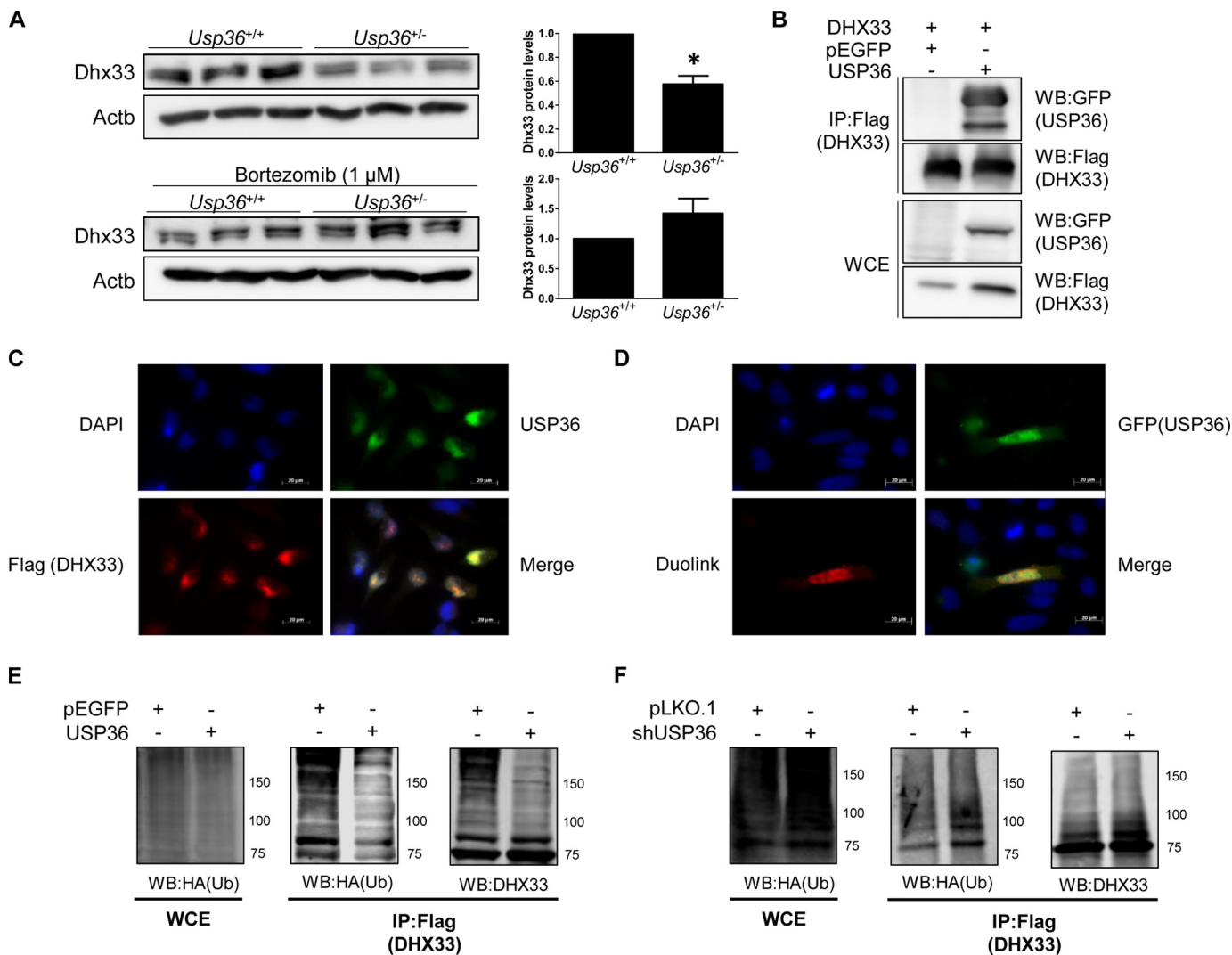
Figure 3. USP36 regulates the ubiquitination levels of DHX33. *A,* Western blot analysis and densitometry quantification of Dhx33 levels in *Usp36*$^{+/+}$ and *Usp36*$^{+/-}$ MEFs, before and after treatment with bortezomib, two-tailed Student's *t* test (*, $p < 0.05$). The densitometry quantification of each band was normalized to the wildtype signal from the same blot to compare the data. *B,* FLAG- and GFP-specific Western blot analyses of FLAG immunoprecipitates (*IP:Flag*) from HEK-293T cells transiently cotransfected with FLAG-tagged DHX33 plus either GFP-USP36 or GFP. *C,* colocalization of USP36 (*green*) and DHX33 (*red*) was analyzed through immunofluorescence analysis. *Scale bar* = 20 μm. *D,* representative fluorescence images showing Duolink fluorescence as USP36 and DHX33 interaction (*red signal*), USP36 (GFP), and merged with DAPI. *Scale bar* = 20 μm. *E,* ubiquitination levels analyzed by Western blot (anti-HA and anti-DHX33) of FLAG immunoprecipitates (*IP:Flag*) from HEK-293T cells transiently cotransfected with FLAG-tagged DHX33 and HA-ubiquitin plus either GFP-USP36 or GFP expression vectors and treated with bortezomib. *F,* DHX33 protein levels and ubiquitination status analyzed by Western blot (anti-HA and anti-DHX33) of FLAG immunoprecipitates (*IP:Flag*) from HEK-293T cells transiently cotransfected with FLAG-tagged DHX33 and HA-ubiquitin plus either pLKO.1 or *USP36*-specific shRNA vectors and treated with bortezomib. *WCE,* whole cell extracts.

and can be visualized by copper(I)-catalyzed azide-alkyne cycloaddition (26). As it is shown in Fig. 4*A*, deficiency of Usp36 at the morula stage decreased OP-Puro incorporation, suggesting an impairment of mRNA translation.

Because DHX33 has also been described as a mediator or rRNA synthesis (21), the role of USP36 in this phenomenon was next analyzed. With this purpose, 45S pre-rRNA levels of USP36-depleted and control HCT116 colorectal cancer cells were quantified by Northern blot analysis, finding that down-regulation of *USP36* significantly decreased 45S pre-rRNA accumulation (Fig. 4, *B* and *C*). Moreover, silencing of *USP36* also caused more alterations in pre-rRNA processing, such as diminished 21S levels (Fig. 4, *B* and *D*), and consequently increased the 28S/18S ratio (Fig. 4*E*). Because these results support a direct role of USP36 in the regulation of rRNA pro-

cessing, the hypothetical impact of *Usp36* down-regulation on the nucleolar structure was investigated by analyzing MEFs processed for electron microscopy. Interestingly, *Usp36*-heterozygous MEFs showed nucleoli significantly larger than wildtype MEFs (Fig. 5*A*). Although *Usp36*-heterozygous MEFs also exhibited an increase in nucleus size (Fig. 5*B*), the ratio of nucleolar to nuclear area was consistently higher when compared with that of wildtype cells (Fig. 5, *C* and *D*). Finally, the effect of *USP36* down-regulation was examined through the meta-analysis of the data derived from a genomewide shRNA screen in 216 cancer cell lines from multiple tumor types (27), finding that the antiproliferative effects of silencing *USP36* correlated positively with the antiproliferative effects of silencing genes involved in translation and ribosome biogenesis (Fig. 5*E*).
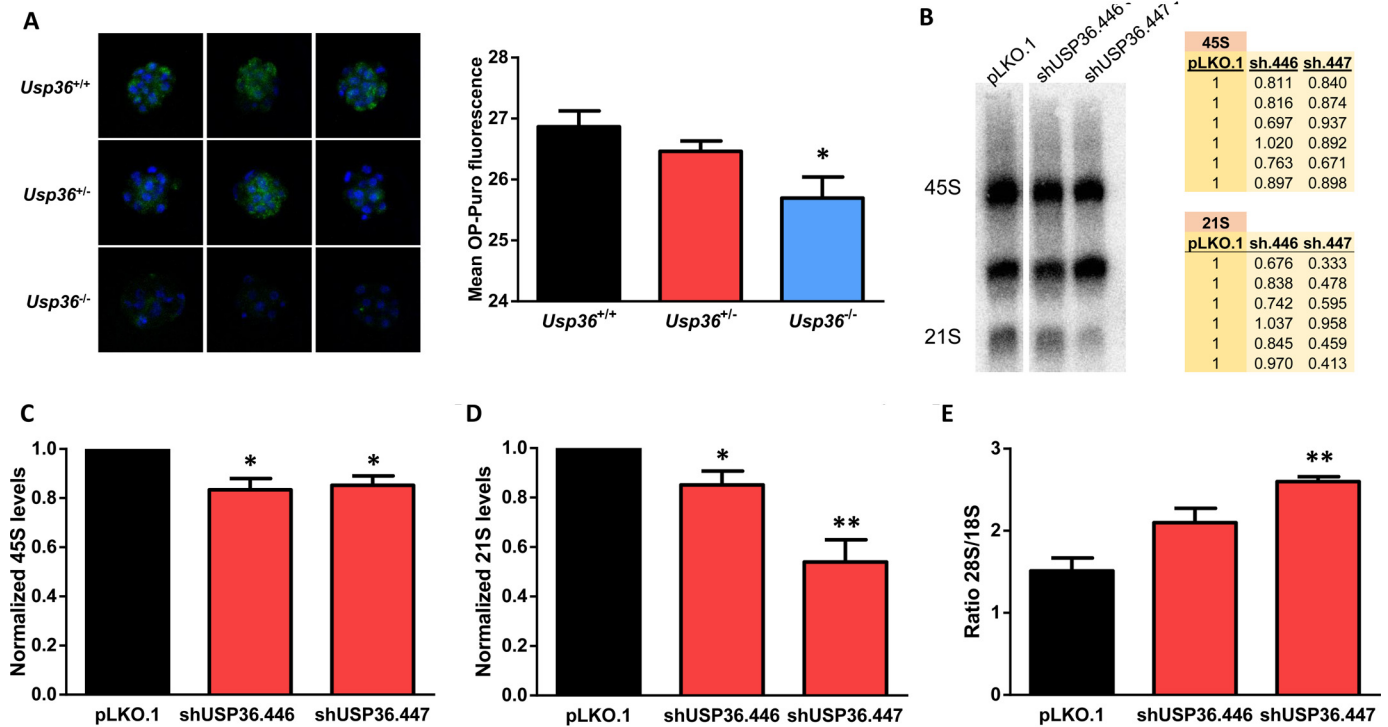
Figure 4. USP36 depletion impairs protein and rRNA synthesis. *A,* representative images of 3.5 dpc embryos incubated with OP-Puro and visualized by fluorescence microscopy after conjugation with Alexa Fluor 488. The *bar graph* represents the quantification of mean fluorescence obtained from 40 embryos at 3.5 dpc. Fluorescence baseline = 20. Data are represented as mean ± S.E. and statistical significance was assessed by using a non-parametric Mann-Whitney-Wilcoxon test (*, $p < 0.05$). *B,* representative image of Northern blot analysis of RNA from HCT116 cells transduced with control (pLKO.1) or two *USP36*-specific shRNAs (shUSP36.446 and shUSP36.447) and densitometry quantification of six technical replicates. The densitometry quantification of each band was normalized to pLKO.1 signal from the same blot to compare the data. *C* and *D,* Northern blot analysis showed that down-regulation of *USP36* decreased the levels of 45S pre-rRNA (*C*) and 21S pre-rRNA (*D*), two-tailed Student's *t* test (*, $p < 0.05$; **, $p < 0.01$). *E,* bioanalyzer experiments demonstrate that down-regulation of USP36 increased the 28S/18S ratio, two-tailed Student's *t* test (**, $p < 0.01$).
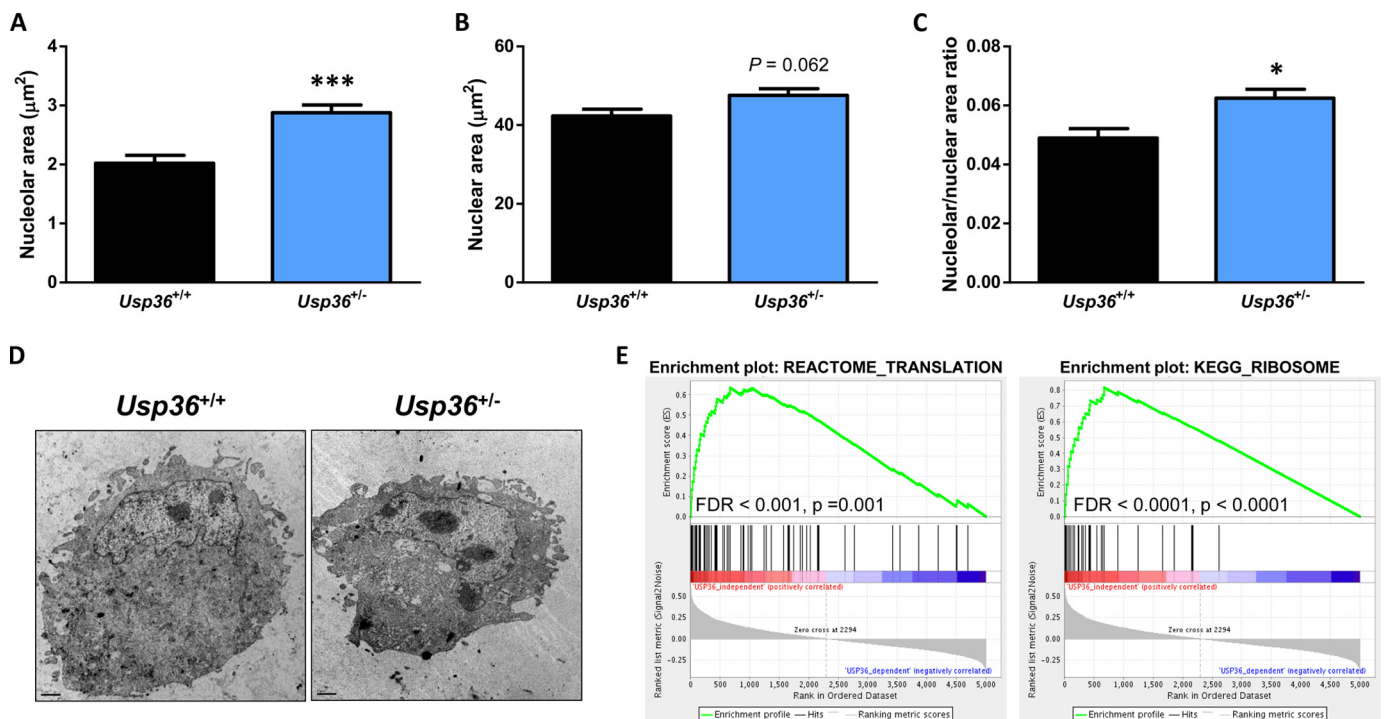

Figure 5. *USP36* down-regulation alters nucleolar structure. *A* and *B,* nucleolar (*A*) and nuclear (*B*) areas of $Usp36^{+/+}$ and $Usp36^{+/-}$ MEFs. *C,* nucleolar area normalized to nuclear area of $Usp36^{+/+}$ and $Usp36^{+/-}$ MEFs. *D,* representative images of MEFs processed for electron microscopy. *E,* GSEA analysis from a genome-wide screen with 216 cancer cell lines from multiple tumor types (Broad Institute Project Achilles) showed that the antiproliferative effects of silencing *USP36* correlated positively with gene sets containing genes involved in translation and ribosome biogenesis. Selected enriched pathways had a relaxed FDR $<$ 0.001 and $p < 0.001$. Data are represented as mean ± S.E. and statistical significance was assessed by using a non-parametric Mann-Whitney-Wilcoxon test (*, $p < 0.05$; ***, $p < 0.001$).
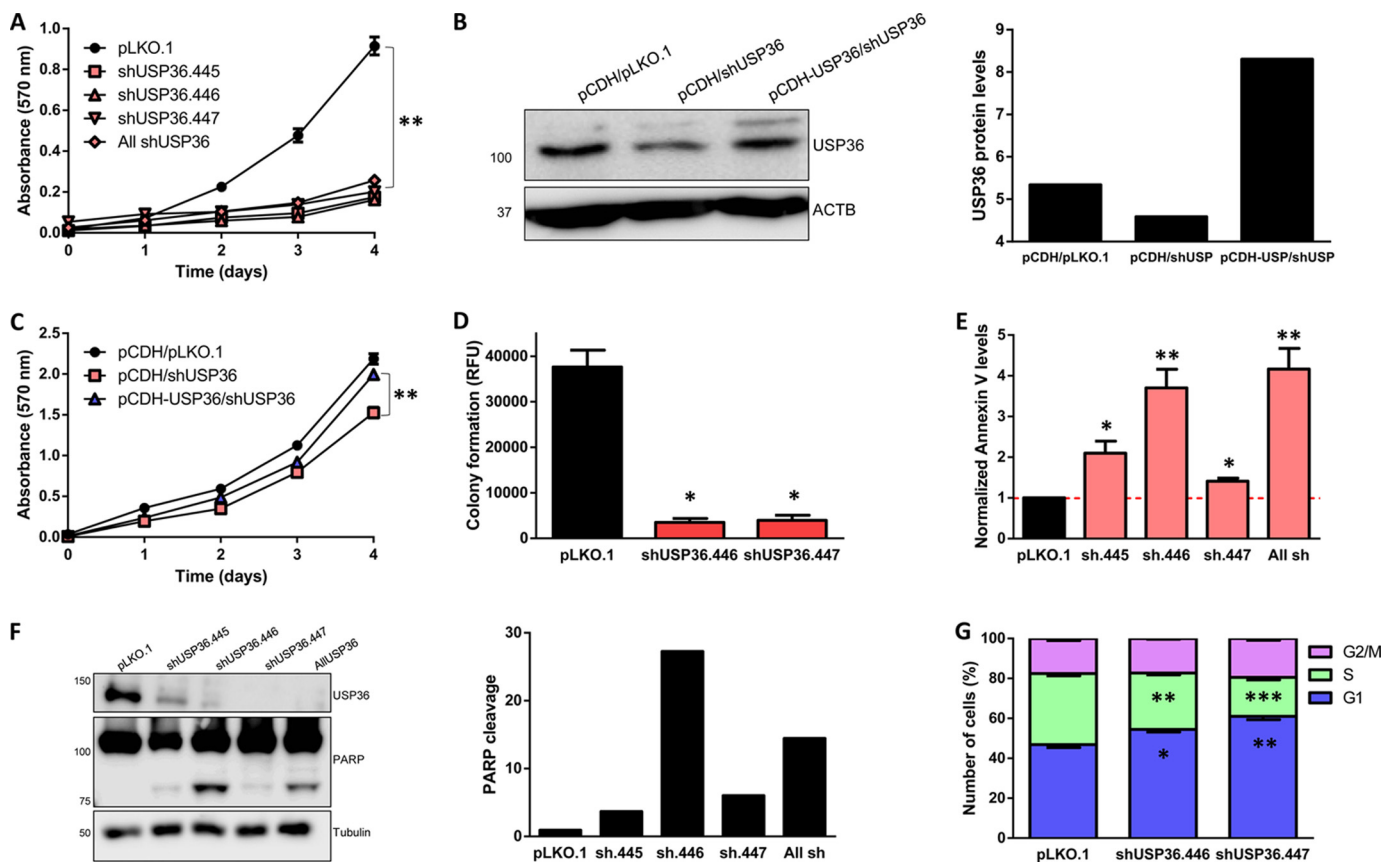
Figure 6. USP36 silencing abrogates HCT116 proliferation. *A*, MTT proliferation assay of HCT116 cell transduced with control (pLKO.1) or three *USP36*-specific shRNAs (shUSP36.445, shUSP36.446, and shUSP36.447) either separately or in combination (all shUSP36). *B*, Western blot analysis and densitometry quantification of USP36 expression in HCT116 cells transduced with USP36-specific shRNA (shUSP36) and/or an shRNA-resistant *USP36* cDNA (pCDH-USP36). *C*, USP36 shRNA effects on HCT116 proliferation were rescued by the overexpression of a *USP36* shRNA-resistant cDNA. *D*, soft agar colony formation assay showing anchorage-independent growth of control and USP36-depleted HCT116 cells. *E*, Annexin V-FITC positive cells were analyzed by flow cytometry in *USP36*-silenced and control cells. The percentage of Annexin V-FITC positive cells of each condition was normalized with that of control cells (pLKO.1). *F*, Western blot analysis and densitometry quantification of HCT116 cells transduced with empty vector and *USP36*-specific shRNAs showing *USP36* down-regulation and apoptosis induction (PARP cleavage). *G*, flow cytometry-based cell cycle analysis showing an increase in G_1 population upon *USP36* down-regulation, two-tailed Student's *t* test (*, $p < 0.05$; **, $p < 0.01$; ***, $p < 0.001$). Data from MTT proliferation, soft agar colony formation, and Annexin V-FITC assays are presented as mean ± S.E. and statistical significance was assessed by using a non-parametric Mann-Whitney-Wilcoxon test (*, $p < 0.05$; **, $p < 0.01$).

Collectively, these results strongly support that USP36, similarly to DHX33, is essential for the regulation of rRNA synthesis and mRNA translation processes, whose optimal function is required during embryonic development. In this sense, any dysfunctional mutation within *Usp36* could lead to a devastating effect, as demonstrated by the finding of preimplantation lethality in *Usp36*-deficient mice.

USP36 depletion induces p53-independent apoptosis and p53-dependent cell cycle arrest

To investigate the mechanistic intricacies underlying the lethality caused by Usp36 depletion, HCT116 colorectal cancer cells were chosen as an experimental model. As a first approach, the proliferation rate of human HCT116 colorectal cancer cells transduced with either control or *USP36*-specific shRNAs was analyzed. As shown in Fig. 6A, USP36 depletion with three independent shRNAs, either separately or in combination, decreased the proliferation rate of HCT116 cells. To demonstrate the absence of noticeable off-target effects, a lentiviral vector encoding a shRNA-resistant *USP36* cDNA was transduced into HCT116 cells. USP36 protein levels were analyzed by Western blot (Fig. 6B). As shown in Fig. 6C, ectopic expression of this cDNA abrogated the effects of the shRNA-mediated USP36 silencing in this cell line, corroborating the specificity of our approach. Moreover, down-regulation of *USP36* in HCT116 cells reduced their ability to grow in soft agar (Fig. 6D). Accordingly, USP36 depletion with three independent shRNAs induced apoptosis, as evidenced by an increase in the percentage of Annexin V-positive cells (Fig. 6E). In agreement with these results, Western blot analysis of PARP cleavage also confirmed apoptosis induction upon *USP36* down-regulation (Fig. 6F), corroborating the results obtained from TUNEL analysis performed in *Usp36*⁻/⁻ morulae. To investigate whether USP36 depletion alters cell cycle progression, the cell cycle profile of wildtype and *USP36*-silenced cells was analyzed by flow cytometry. Interestingly, *USP36* down-regulation induced an increased accumulation of cells in the G_1 phase compared with controls, suggesting a G_1 cell cycle arrest (Fig. 6G). Altogether, these results indicate that USP36 deficiency alters cell proliferation, inducing both apoptosis and cell cycle arrest.

To determine whether p53 plays a role in the apoptotic response induced by *USP36* silencing, *USP36* was next down-regulated in p53-deficient HCT116 cells. Remarkably, p53 deficiency did not rescue the cell lethality caused by *USP36* down-
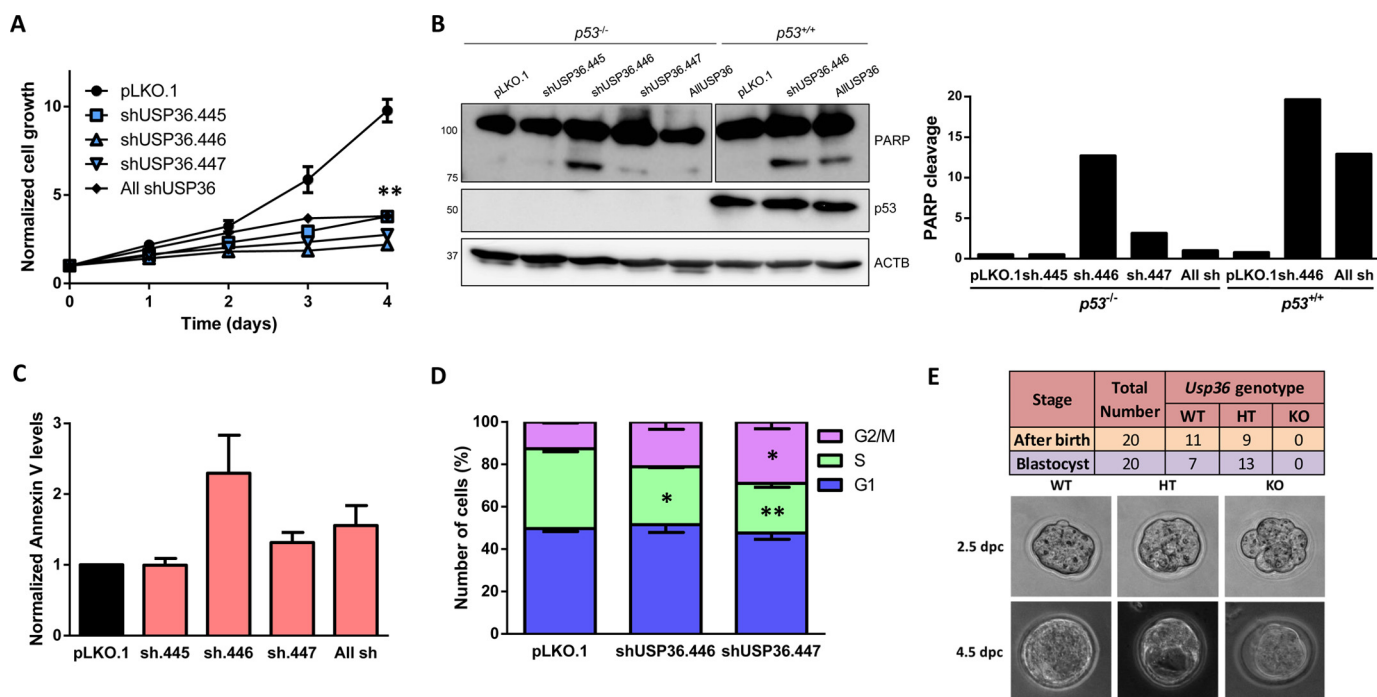
Figure 7. *USP36* down-regulation induces p53-independent apoptosis and p53-dependent cell cycle arrest. *A,* MTT proliferation assay of HCT116 $p53^{-/-}$ cells stably transduced with control and *USP36*-specific shRNAs. Absorbance of each day is normalized with respect to absorbance of day 0. Data are presented as mean ± S.E. and statistical significance was assessed by using a non-parametric Mann-Whitney-Wilcoxon test (**, $p < 0.01$). *B,* Western blot analysis and densitometry quantification of PARP cleavage as an indicator of apoptosis in protein extracts of HCT116 $p53^{+/+}$ and $p53^{-/-}$ cells transduced with control and *USP36*-specific shRNAs. *C,* Annexin V-FITC positive cells levels of USP36-silenced and control cells. The percentage of Annexin V-FITC positive cells of each condition was normalized with respect to that of control cells (pLKO.1). *D,* flow cytometry-based cell cycle analysis of wildtype and *USP36*-silenced HCT116 $p53^{-/-}$ cells, two-tailed Student's *t* test (*, $p < 0.05$; **, $p < 0.01$). *E,* distribution of genotyped offspring and embryos from $Usp36^{+/-}$ $p53^{-/-}$ intercrosses and representative images of embryos from intercrosses of $Usp36^{+/-}$ $p53^{-/-}$ mice obtained at 2.5 dpc (morulae) and cultured *in vitro* for 48 h (blastocysts, 4.5 dpc).

regulation (Fig. 7*A*). Furthermore, USP36-depleted cells underwent some degree of apoptosis even in the absence of p53 (Fig. 7, *B* and *C*), indicating that *USP36* down-regulation induces a p53-independent apoptotic response. By contrast, a significant increase in G_1 population cells was not observed after *USP36* silencing, although the accumulation of cells in G_2 phase of the cycle was noteworthy (Fig. 7*D*). Altogether, these results suggest that USP36 depletion induces both p53-dependent cell cycle arrest and p53-independent apoptosis. Next, we decided to investigate the possible relevance of these mechanisms in the embryonic lethality caused by Usp36 deficiency. With this purpose, $p53^{-/-}$ mice were crossed with $Usp36^{+/-}$ mice, which were then inbred to obtain $Usp36^{+/-}$ $p53^{-/-}$ mice. Finally, these mice were intercrossed and the resulting offspring genotyped and analyzed. As shown in Fig. 7*E*, no $Usp36^{-/-}$ $p53^{-/-}$ mice were detected at weaning. Next, 2.5 dpc embryos were collected and cultured *in vitro* for 2 days to obtain blastocysts. However, no $Usp36^{-/-}$ $p53^{-/-}$ blastocysts were found. By contrast, we obtained some $Usp36^{-/-}$ $p53^{-/-}$ arrested morulae (Fig. 7*E*). Therefore, these results demonstrate that $Usp36^{-/-}$ embryos exhibit preimplantation lethality at the morula stage in a p53-independent manner.

Finally, to further evaluate if *DHX33* down-regulation mimics the biological effect caused by USP36 depletion, an empty vector (pLKO.1) and two independent *DHX33*-specific shRNAs (shDHX33.61 and shDHX33.62) were transduced into HCT116 cells. As observed upon USP36 targeting, silencing of *DHX33* in HCT116 cells significantly reduced their prolifera-

tion rate (Fig. 8*A*). Western blot analyses were performed to analyze DHX33 protein levels (Fig. 8*B*). Furthermore, cells transduced with *DHX33*-specific shRNAs showed an increase in apoptosis, as evidenced by analyzing both PARP cleavage (Fig. 8*C*) and the percentage of Annexin V-FITC positive cells (Fig. 8*D*). Altogether, these results corroborate that *DHX33* down-regulation phenocopies *USP36* silencing in human cancer cells, and support our hypothesis that USP36 is essential for cell viability due to its critical role in rRNA processing and protein synthesis by regulating the ubiquitination levels of DHX33.

Discussion

In this work, we have generated an *Usp36*-deficient mouse model that shows a lethal phenotype during the preimplantation stage, demonstrating the essentiality of this deubiquitinase for embryonic development. Moreover, we have evaluated the functional role of USP36 by analyzing the proteomic profile of wildtype and heterozygous mice for this deubiquitinase. Our studies have shown that USP36 directly interacts with DHX33, a DEAH-box RNA helicase involved in RNA polymerase I-mediated transcription and mRNA translation initiation (20, 21). Furthermore, we have described for the first time the regulatory role of USP36 on the ubiquitination levels and stability of DHX33.

So far, many nucleolar proteins associated with RNA processing have been described as essential for proliferation and survival of human cells (28, 29). Furthermore, several mouse
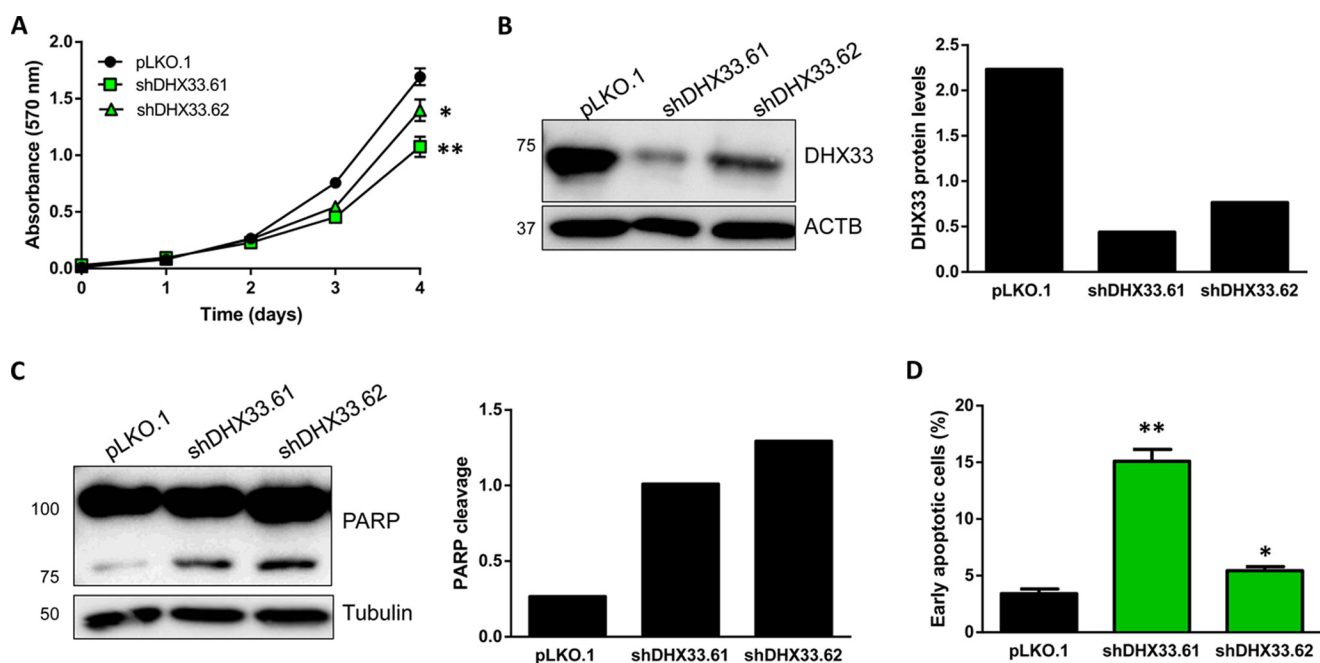
Figure 8. shRNA-mediated down-regulation of *DHX33* phenocopies *USP36* silencing. *A,* MTT proliferation assay of the HCT116 cells transduced with control (pLKO.1) or two *DHX33*-specific shRNAs (shDHX33.61 and shDHX33.62). *B,* Western blot analysis and densitometry quantification of DHX33 expression in HCT116 cells used in *A*. *C,* Western blot analysis of PARP cleavage as an indicator of apoptosis in protein extracts of HCT116 cells transduced with control (pLKO.1) or *DHX33*-specific shRNAs (shDHX33.61 and shDHX33.62). *D,* flow cytometry assay showing the percentage of Annexin V-FITC positive cells as an indicator of early apoptosis.

models deficient for ribosome biogenesis regulators also show embryonic lethality at the preimplantation stage. Thus, *Pescadillo*-deficient mouse embryos arrest at the morula stage of development (30). Similarly, mice carrying a truncated mutation in the gene encoding polypeptide B of RNA polymerase I display nucleolus disruption and apoptotic cell death at the morula stage (31). Furthermore, fibrillarin-deficient mouse embryos also die beyond the morula stage (32) and *Surf6* knockdown by RNAi results in development arrest at the morula stage (33). Finally, UBF and nucleostemin are also essential for embryo development beyond morula (34, 35). The results derived from our study have demonstrated *in vivo* that Usp36 is a nucleolar protein related to ribosome biogenesis and RNA processing regulation. Thus, OP-Puro treatment has demonstrated that *Usp36*-deficient morulae exhibit impaired protein synthesis, highlighting the importance of Usp36 in this cellular process. Moreover, Northern blot analysis has shown that USP36 deficiency induce aberrations in rRNA synthesis. According to USP36 nucleolar activity, *Usp36*-heterozygous MEFs exhibit alterations in their nucleolar structure, a phenomenon that has been tightly correlated with ribosome biogenesis aberrations (36). In agreement with these results, meta-analysis of a genome-scale shRNA screen of 216 cancer cell lines of multiple histological origins has revealed that the anti-proliferative effects of silencing *USP36* and genes involved in translation and ribosome biogenesis positively correlate, supporting the direct role of this deubiquitinating enzyme in both physiological processes. Altogether, these results strongly support the critical role of USP36 in rDNA transcription and mRNA translation, at least in part, by regulating the stability of DHX33. However, further studies on other putative USP36

substrates will be required to completely understand its functional role in these biological processes.

It is widely accepted that inappropriate ribosome biogenesis, perturbed rRNA processing, and ribosome assembly induce apoptosis and block cell proliferation (36, 37). Accordingly, the results obtained in TUNEL experiments have revealed that *Usp36* deficiency induces apoptosis at the preimplantation stage of development. Furthermore, we have demonstrated that *USP36* down-regulation with specific shRNAs reduces the proliferation and the anchorage-independent growth of human cancer cells, through both p53-dependent and -independent mechanisms. Thus, even in the absence of p53, *USP36* ablation leads to cell death, both in human colorectal cancer cells and in preimplantation mouse embryos. Additionally, we have demonstrated that reducing DHX33 protein levels by an USP36-independent mechanism also abrogates the proliferation of HCT116 cells and increases their apoptotic rate, supporting our hypothesis that the USP36 role in regulating DHX33 stability is critically required for cell viability.

In summary, the generation of *Usp36*-deficient mice has allowed us to identify USP36 as an essential gene for cell and organism viability. We describe for the first time the regulatory role of USP36 on the ubiquitination levels and stability of DEAH-box RNA helicase DHX33, which constitutes a new mechanism of USP36 functional implication in rRNA processing and protein synthesis.

Experimental procedures

Generation of Usp36⁻/⁻ mice and genotyping

Usp36-mutant embryonic stem cells were purchased from EUKOMP (EUCE00141e03, from the 129P2/OlaHsd mouse

strain). Two different clones of targeted embryonic stem cells were microinjected into C57BL/6 mouse blastocysts to produce chimeric mice that were then subsequently crossed with C57BL/6 mice to generate *Usp36*-heterozygous mice. *Usp36*-knockout first allele was identified by Southern blotting and PCR. For Southern blot experiments, the recombinant allele (3,640 bp) was detected by a specific probe in BclI-digested genomic DNA. For PCR genotyping, genomic DNA from tail samples was used under the following conditions: denaturation at 94 °C for 30 s, annealing at 60 °C for 30 s, and extension at 72 °C for 30 s, 30 cycles. The following primers were used for genotyping: wildtype-specific forward 5′-ccaggtctctcaaggactagga-3′, mutation-specific forward 5′-gaatgaaagaccccacctgtag-3′, and common reverse 5′-aggatgccaaagagcatgtagt-3′. p53-deficient mice were kindly provided by Dr. M. Serrano.

Cell culture

Cancer cell lines HEK-293T, HeLa, and HCT116 were purchased from the American Type Culture Collection. Cells were routinely maintained in Dulbecco's modified Eagle's medium containing 10% fetal bovine serum, 100 units/ml of penicillin, and 100 μg/ml of streptomycin (Life Technologies). HCT116 $p53^{-/-}$ cells were kindly provided by Dr. B. Vogelstein. MEFs were extracted and cultured as previously described (38).

Cell cycle analysis

HCT116 cells transduced with control and *USP36*-specific shRNAs were washed twice with PBS and permeabilized with 1 ml of 70% ethanol at −20 °C added drop by drop. After 30 min on ice, cells were washed twice in PBS and resuspended in 1 ml of 20 μg/ml of propidium iodide (PI), 200 μg/ml of RNase in PBS for 15 min in the dark at room temperature. Finally, the cell cycle was analyzed by flow cytometry (10,000 events per sample, Cytomics FC500, Beckman Coulter).

shRNA lentiviral infection

USP36-specific shRNAs, *DHX33*-specific shRNAs, and empty vector (pLKO.1) (Open Biosystems, Thermo Scientific) were packaged in HEK-293T cells using a vesicular stomatitis virus glycoprotein-based package system. Viral supernatant was collected at 24 h and added in a 1:3 dilution to previously seeded HCT116 cells, supplemented with 5 mg/ml of Polybrene (Millipore). HCT116 stably transduced cells were selected with puromycin at a final concentration of 1 μg/ml.

Cell-proliferation assay

To quantify cell proliferation, 5,000 cells per well were seeded ($n = 6$) into 96-well plates and a Cell Titer 96 NonRadioactive cell proliferation kit was used following the manufacturer's instructions (Promega Corp.).

shRNA-resistant USP36 expression

Silent mutations were introduced into the shUSP36.447 target sequence of *USP36* cDNA cloned in pCDH-puro, using the Q5® Site-directed Mutagenesis Kit (New England

Biolabs) and the primers: 5′-ggcttacagccgacatcttgccatcccaggt-3′ and 5′-aagacgccatcgaagacagcagacaggcccgga-3′. Lentiviral particles were packaged as described above. HCT116 cells were simultaneously transduced with the *USP36*-specific shRNAs shUSP36.447 and the shRNA-resistant *USP36* cDNA or the empty vector and their proliferation was assessed without prior antibiotic selection. It is noteworthy that HCT116 cells were simultaneously transduced with two different plasmids (*USP36*-specific shRNAs and a shRNA-resistant *USP36* cDNA clone), which shared the same antibiotic resistance, leading to a smaller fraction of silenced cells. Therefore, the anti-proliferative effect of this experiment was smaller and observed later when compared with that of Fig. 6A.

Soft agar colony formation

1,000 cells per well were seeded, maintained during 8 days at 37 °C and 5% CO_2 and anchorage-independent growth was analyzed with CytoSelect™ 96-Well In Vitro Tumor Sensitivity Assay kit (Cell Biolabs), following the manufacturer's instructions.

Northern blot

A total of 10 μg of denatured RNA was separated by electrophoresis on 1.2% agarose gels and transferred to Hybond N+ (Amersham Biosciences). Blots were prehybridized at 42 °C for 3 h in 50% formamide, 5× SSPE (1× = 150 mm NaCl, 10 mm NaH_2PO_4, 1 mm EDTA, pH 7.4), 10× Denhardt's solution, 1.4% SDS, and 100 μg/ml of denatured herring sperm DNA. Then, the blot was hybridized with a genomic DNA probe synthetized by PCR using the following primers: 5′-gagaactcgggagggagac-3′ and 5′-gaccctcgagacgccta-3′ for 24 h under the same conditions. Blots were washed twice with 2× SSC, 0.05% SDS for 20 min at room temperature. Finally, blots were washed three times with 0.1× SSC, 0.1% SDS for 20 min at 50 °C and exposed to autoradiography.

Western blot analysis

Western blot analyses were performed as previously described (39) using the following antibodies: anti-USP36 antibody (14783-1-AP, Proteintech), anti-PARP (9542, Cell Signaling), anti-p53 (sc-126, Santa Cruz Biotechnology), anti-DHX33 (NB100−2581, Novus Biologicals), anti-FLAG (2368, Cell Signaling), anti-β-actin (AC-15, Sigma), anti-α-tubulin (T6074, Sigma), and anti-HA (11867423001, Roche Applied Science).

Annexin V analysis and PI staining

HCT116 cells transduced with either control, *USP36*-specific shRNAs or *DHX33*-specific shRNAs, were labeled with Annexin V-FITC (Inmunostep) and PI for 10 min in the dark. The percentage of positive Annexin V cells was analyzed by Flow Cytometry (15,000 events per sample).

TUNEL and OP-Puro treatment

Embryos derived from *Usp36*-heterozygous mice intercrosses were flushed at day 2.5 dpc and cultured overnight. For OP-Puro experiments, embryos at 3.5 dpc were incubated with 50 μM OP-Puro for 1 h at 37 °C. Then, they were washed with

PBS and fixed in 4% paraformaldehyde in PBS for 5 min at room temperature. They were subsequently washed with PBS and permeabilized in 0.1% Triton X-100, 0.1% sodium citrate for 2 min. Embryos were washed with 2% BSA in PBS and the azide-alkyne cycloaddition was performed using the Click-iT Cell Reaction Buffer Kit (Life Technologies) and azide conjugated to Alexa Fluor 488 (Life Technologies) at a 5 μM final concentration. After 30 min of incubation at room temperature, morulae were washed with 2% BSA in PBS and images were taken using a Leica TCS-SP8X laser confocal microscope (HCX PL FLU-OTAR L ×20/0.40 DRY, zoom 2.70). For TUNEL staining, embryos were fixed and permeabilized as for OP-Puro experiments. Embryos were then washed with PBS and incubated with terminal deoxynucleotidyltransferase and fluorescein-labeled dUTP for terminal deoxynucleotidyltransferase-mediated dUTP-biotin nick end labeling (TUNEL) (In Situ Cell Death Detection kit; Roche Applied Science) at 37 °C for 1 h. Embryos were washed with PBS before they were analyzed with a Leica DMI6000B inverted microscope and photographed with a Leica DFC480 camera (Leica Image Manager software). After analysis, embryos were individually transferred into PCR tubes and processed for genotyping.

Electron microscopy

MEFs were collected and fixed in 3% glutaraldehyde in cacodylate buffer. Then, they were transferred into agar, and post-fixed with 1% osmium tetroxide for 1 h. We then rinsed the samples 3 times in Sorensen's buffer and agar blocks were dehydrated in graded ethanol and infiltrated in 50% propylene oxide, 50% resin. After 1 h, samples were embedded in a resin-based mold for polymerization overnight at 37 °C. Finally, ultra-thin sections (85 nm) were taken from each experiment and analyzed on a Jeol (JEM-1011) transmission electron microscope at 60 kV.

Sample preparation for mass spectrometry

Protein samples were prepared by triplicate from wildtype and *Usp36*-heterozygous MEFs in 150-mm dishes. Cells were washed twice with ice-cold PBS, scraped in PBS, spun down, and lysed in SDS buffer (2% SDS, 150 mM NaCl, 50 mM HEPES pH 8.0, with added complete protease inhibitors (Roche Applied Science) and PhosSTOP phosphatase inhibitors (Roche Applied Science). 25-Guage needles were used to homogenize the cell pellet and lyse it. Cell debris was spun down for 15 min at 13,000 × *g* at 4 °C. Protein concentration was determined using the BCA assay (Thermo Fisher Scientific). To reduce and alkylate the disulfide bonds, 300 μg of lysate was incubated with 5 mM tris(2-carboxyethyl)phosphine for 30 min and 14 mM iodoacetamide for 30 min at room temperature in the dark. Proteins were precipitated using methanol/chloroform precipitation and resuspended in 8 M urea buffer (8 M urea, 50 mM HEPES, pH 8.0, 1 mM CaCl$_2$). Protein extracts were diluted to 4 M urea using 50 mM HEPES, pH 8.0, and digested for 2 h at 37 °C with LysC (Wako) at a 1:250 LysC/protein ratio. Then, diluted to 2 M urea, and incubated overnight at 37 °C with LysC. The next day, urea was further diluted to 1 M and trypsin (Promega) was added at a 1:50 trypsin/protein ratio for 6 h at 37 °C. The proteolytic peptides were then

acidified with formic acid (FA) to a pH of <2 and desalted using Sep-Pak C$_{18}$ solid-phase extraction cartridges (Waters), following the manufacturer's protocol. Dried peptides were resuspended in 200 mM HEPES, pH 8.0, the concentration was determined using the micro-BCA protein assay (Thermo Fisher Scientific) and the isobaric labeling of the peptides was performed using 6-plex TMT reagents (Thermo Fisher Scientific). Thus, 100 μg of peptides at 1 μg/μl were labeled with 0.2 mg of each TMT reagent (previously dissolved in acetonitrile (ACN)) for 2 h at room temperature. Finally, the reactions were quenched with 0.3% hydroxylamine (Sigma) at room temperature for 15 min. The resultant labeled peptides were combined equally and ACN diluted to 3% with 3% FA (final pH should be <2). The peptides were desalted again with a Sep-Pak C$_{18}$ column and dried down in the SpeedVac. The peptides were then subjected to basic-pH reverse-phase HPLC fractionation as described (40) and fractionated into 24 fractions. Half of them were dried down in the SpeedVac, dissolved in 3% FA, 3% ACN, desalted via StageTip, dried again in the SpeedVac, and resuspended in 10 μl of 3% FA, 3% ACN just before mass spectrometry analysis.

Mass spectrometry analysis

All spectra were acquired on an Orbitrap Fusion (Thermo Fisher Scientific) coupled to a Proxeon EASY-nLC II LC pump (Thermo Fisher Scientific) as described previously (40). Briefly, peptides were separated on an in-house packed column with ~35 cm of GP-18 resin (1.8 μm, 200 Å; Sepax) using a gradient of 135 min from 6 to 26% ACN in 0.125% FA at a flow rate of ~350 nl/min. The scan sequence in the mass spectrometer began with FTMS1 spectra (resolution of 120 k; mass range 400–1400 *m/z*; automatic gain control (AGC) target 2×10^5, maximum injection time of 100 ms) followed by the selection of the 10 most intense ions for MS/MS with a dynamic exclusion of 90 s. ITMS2 spectra were collected in the ion trap with a maximum injection time of 150 ms with an AGC target 4×10^3 and CID collision energy of 35%. FTMS3 spectra were collected using the multi-notch method previously described (41). Briefly, to create TMT reporter ions, a synchronous-precursor-selection-MS3 scan was collected on the top 10 most intense ions in the MS2 spectrum. Synchronous-precursor-selection-MS3 precursors were fragmented by high energy collision-induced dissociation and analyzed using the Orbitrap (NCE = 55%, AGC = 5×10^4, maximum injection time = 150 ms, and resolution = 15 K). The data analysis were performed with a SEQUEST-based in-house software pipeline (42). In short, mass spectra were searched against the mouse Uniprot database (February 2014) and a reverse decoy database. Precursor ion tolerance was set at 20 ppm and product ion tolerance at 0.9 Da. Addition of a TMT tag (+229.1629 Da) on lysine residues and peptide N termini, and cysteine carbamidomethylation (+57.0215 Da) were added as static modifications, and methionine oxidation (+15.9949 Da) was set as a variable modification. Peptide-spectrum matches were adjusted to a 1% false discovery rate using a linear discriminant analysis (42), quantified by extracting the signal to noise ratio and proteins were further collapsed to a final protein level false discovery rate of

1% ([40, 41]). Statistical analysis was performed using two-tailed Student's *t* test.

Immunoprecipitation

HEK-293T cells were transfected with pLVX–FLAG–DHX33 and pEGFP–USP36 or pEGFP empty vector and immunoprecipitation was performed as previously described ([43]). For ubiquitination experiments, HEK-293T cells were transfected with HA–ubiquitin and pLVX–FLAG–DHX33, together with pEGFP/pEGFP-USP36 or pLKO.1/*USP36*-specific shRNA plasmids, treated with 500 nM bortezomib during 16 h and lysed with RIPA buffer (100 mM Tris-HCl, pH 7.4, 150 mM NaCl, 10 mM EDTA, 1% sodium deoxycholate, 1% Triton X-100, 0.1% SDS and protease and phosphatase inhibitors). Then, protein extracts were precleared for 4 h at 4 °C with Dynabeads™ Protein G (Life Technologies), released from beads and incubated in rotation with anti-FLAG antibody overnight at 4 °C. Beads were next washed three times with co-IP buffer and incubated in rotation with antibody-conjugated protein extracts 4 h at room temperature. Immunoprecipitates and input samples were resolved by SDS-PAGE and immunostained with anti-HA and anti-DHX33 antibodies.

P-LISA and imunofluorescent staining

The interaction between USP36 and DHX33 was detected using P-LISA (Sigma). HeLa cells were seeded on coverslips and co-transfected with pEGFP–USP36 and pLVX–FLAG–DHX33 plasmids. After 24 h, coverslips were fixed with 4% paraformaldehyde for 10 min, permeabilized with 0.5% Triton X-100 for 5 min, and blocked with Duolink blocking buffer for 30 min at 37 °C in a humidity chamber. Incubation with anti-FLAG and anti-USP36 antibodies was carried out overnight at 4 °C in a humidity chamber. Incubation with secondary probes, ligation, and amplification steps were all performed according to the manufacturer's instructions. For immunofluorescent staining, HeLa cells transfected with pEGFP–USP36 and pLVX–FLAG–DHX33 plasmids were fixed, permeabilized as indicated above, and blocked with 15% goat serum for 1 h at room temperature. Incubation with anti-FLAG and anti-GFP antibodies was performed overnight at 4 °C in a humidity chamber. Secondary antibody incubation was carried out 1 h at room temperature. Then, cells were washed twice with PBS for 5 min and coverslips were mounted with ProLong™ Gold Antifade Mountant with DAPI (Invitrogen, Thermo Fisher Scientific). Positive cells were visualized in an Axioplan-2 fluorescence microscope (Zeiss) under a ×100 oil immersion objective.

GSEA

Gene Set Enrichment Analysis (GSEA) was performed as described ([44]) using GSEA release 2.06 and MSigDB release 2.5 (http://www.broadinstitute.org/gsea/index.jsp).[4] Selected enriched pathways had a relaxed FDR < 0.001 and $p < 0.005$.

---

[4] Please note that the JBC is not responsible for the long-term archiving and maintenance of this site or any other third party hosted site.

References

1. Clague, M. J., Heride, C., and Urbé, S. (2015) The demographics of the ubiquitin system. *Trends Cell Biol.* **25,** 417–426 CrossRef Medline
2. Komander, D., Clague, M. J., and Urbé, S. (2009) Breaking the chains: structure and function of the deubiquitinases. *Nat. Rev. Mol. Cell Biol.* **10,** 550–563 CrossRef Medline
3. Ronau, J. A., Beckmann, J. F., and Hochstrasser, M. (2016) Substrate specificity of the ubiquitin and Ubl proteases. *Cell Res.* **26,** 441–456 CrossRef Medline
4. Ciechanover, A. (2015) The unravelling of the ubiquitin system. *Nat. Rev. Mol. Cell Biol.* **16,** 322–324 CrossRef Medline
5. Fraile, J. M., Quesada, V., Rodríguez, D., Freije, J. M., and López-Otin, C. (2012) Deubiquitinases in cancer: new functions and therapeutic options. *Oncogene* **31,** 2373–2388 CrossRef Medline
6. Reyes-Turcu, F. E., Ventii, K. H., and Wilkinson, K. D. (2009) Regulation and cellular roles of ubiquitin-specific deubiquitinating enzymes. *Annu. Rev. Biochem.* **78,** 363–397 CrossRef Medline
7. Clague, M. J., Barsukov, I., Coulson, J. M., Liu, H., Rigden, D. J., and Urbé, S. (2013) Deubiquitylases from genes to organism. *Physiol. Rev.* **93,** 1289–1315 CrossRef Medline
8. Quesada, V., Ordóñez, G. R., Sánchez, L. M., Puente, X. S., and López-Otin, C. (2009) The Degradome database: mammalian proteases and diseases of proteolysis. *Nucleic Acids Res.* **37,** D239–D243 CrossRef Medline
9. Wang, Z., Zhang, H., Liu, J., Cheruiyot, A., Lee, J. H., Ordog, T., Lou, Z., You, Z., and Zhang, Z. (2016) USP51 deubiquitylates H2AK13,15ub and regulates DNA damage response. *Genes Dev.* **30,** 946–959 CrossRef Medline
10. Ashton-Beaucage, D., Lemieux, C., Udell, C. M., Sahmi, M., Rochette, S., and Therrien, M. (2016) The deubiquitinase USP47 stabilizes MAPK by counteracting the function of the N-end rule ligase POE/UBR4 in *Drosophila*. *PLos Biol.* **14,** e1002539 CrossRef Medline
11. Endo, A., Kitamura, N., and Komada, M. (2009) Nucleophosmin/B23 regulates ubiquitin dynamics in nucleoli by recruiting deubiquitylating enzyme USP36. *J. Biol. Chem.* **284,** 27918–27923 CrossRef Medline
12. Endo, A., Matsumoto, M., Inada, T., Yamamoto, A., Nakayama, K. I., Kitamura, N., and Komada, M. (2009) Nucleolar structure and function are regulated by the deubiquitylating enzyme USP36. *J. Cell Sci.* **122,** 678–686 CrossRef Medline
13. Taillebourg, E., Gregoire, I., Viargues, P., Jacomin, A. C., Thevenon, D., Faure, M., and Fauvarque, M. O. (2012) The deubiquitinating enzyme USP36 controls selective autophagy activation by ubiquitinated proteins. *Autophagy* **8,** 767–779 CrossRef Medline
14. Kim, M. S., Ramakrishna, S., Lim, K. H., Kim, J. H., and Baek, K. H. (2011) Protein stability of mitochondrial superoxide dismutase SOD2 is regulated by USP36. *J. Cell Biochem.* **112,** 498–508 CrossRef Medline

ASBMB

J. Biol. Chem. (2018) 293(6) 2183–2194 **2193**

15. Buszczak, M., Paterno, S., and Spradling, A. C. (2009) Drosophila stem cells share a common requirement for the histone H2B ubiquitin protease scrawny. *Science* **323,** 248–251 CrossRef Medline

16. Sun, X. X., He, X., Yin, L., Komada, M., Sears, R. C., and Dai, M. S. (2015) The nucleolar ubiquitin-specific protease USP36 deubiquitinates and stabilizes c-Myc. *Proc. Natl. Acad. Sci. U.S.A.* **112,** 3734–3739 Medline

17. Richardson, L. A., Reed, B. J., Charette, J. M., Freed, E. F., Fredrickson, E. K., Locke, M. N., Baserga, S. J., and Gardner, R. G. (2012) A conserved deubiquitinating enzyme controls cell growth by regulating RNA polymerase I stability. *Cell Rep* **2,** 372–385 CrossRef Medline

18. Peltonen, K., Colis, L., Liu, H., Trivedi, R., Moubarek, M. S., Moore, H. M., Bai, B., Rudek, M. A., Bieberich, C. J., and Laiho, M. (2014) A targeting modality for destruction of RNA polymerase I that possesses anticancer activity. *Cancer Cell* **25,** 77–90 CrossRef Medline

19. Bourgeois, C. F., Mortreux, F., and Auboeuf, D. (2016) The multiple functions of RNA helicases as drivers and regulators of gene expression. *Nat. Rev. Mol. Cell Biol.* **17,** 426–438 CrossRef Medline

20. Zhang, Y., You, J., Wang, X., and Weber, J. (2015) The DHX33 RNA helicase promotes mRNA translation initiation. *Mol. Cell Biol.* **35,** 2918–2931 CrossRef Medline

21. Zhang, Y., Forys, J. T., Miceli, A. P., Gwinn, A. S., and Weber, J. D. (2011) Identification of DHX33 as a mediator of rRNA synthesis and cell growth. *Mol. Cell Biol.* **31,** 4676–4691 CrossRef Medline

22. Söderberg, O., Gullberg, M., Jarvius, M., Ridderstråle, K., Leuchowius, K. J., Jarvius, J., Wester, K., Hydbring, P., Bahram, F., Larsson, L. G., and Landegren, U. (2006) Direct observation of individual endogenous protein complexes in situ by proximity ligation. *Nat. Methods* **3,** 995–1000 CrossRef Medline

23. Sowa, M. E., Bennett, E. J., Gygi, S. P., and Harper, J. W. (2009) Defining the human deubiquitinating enzyme interaction landscape. *Cell* **138,** 389–403 CrossRef Medline

24. Huttlin, E. L., Ting, L., Bruckner, R. J., Gebreab, F., Gygi, M. P., Szpyt, J., Tam, S., Zarraga, G., Colby, G., Baltier, K., Dong, R., Guarani, V., Vaites, L. P., Ordureau, A., Rad, R., *et al.* (2015) The BioPlex Network: a systematic exploration of the human interactome. *Cell* **162,** 425–440 CrossRef Medline

25. Reed, B. J., Locke, M. N., and Gardner, R. G. (2015) A conserved deubiquitinating enzyme uses intrinsically disordered regions to scaffold multiple protein interaction sites. *J. Biol. Chem.* **290,** 20601–20612 CrossRef Medline

26. Liu, J., Xu, Y., Stoleru, D., and Salic, A. (2012) Imaging protein synthesis in cells and tissues with an alkyne analog of puromycin. *Proc. Natl. Acad. Sci. U.S.A.* **109,** 413–418 CrossRef Medline

27. Cowley, G. S., Weir, B. A., Vazquez, F., Tamayo, P., Scott, J. A., Rusin, S., East-Seletsky, A., Ali, L. D., Gerath, W. F., Pantel, S. E., Lizotte, P. H., Jiang, G., Hsiao, J., Tsherniak, A., Dwinell, E., *et al.* (2014) Parallel genome-scale loss of function screens in 216 cancer cell lines for the identification of context-specific genetic dependencies. *Sci. Data* **1,** 140035 CrossRef

28. Wang, T., Birsoy, K., Hughes, N. W., Krupczak, K. M., Post, Y., Wei, J. J., Lander, E. S., and Sabatini, D. M. (2015) Identification and characterization of essential genes in the human genome. *Science* **350,** 1096–1101 CrossRef Medline

29. Blomen, V. A., Máájek, P., Jae, L. T., Bigenzahn, J. W., Nieuwenhuis, J., Staring, J., Sacco, R., van Diemen, F. R., Olk, N., Stukalov, A., Marceau, C., Janssen, H., Carette, J. E., Bennett, K. L., Colinge, J., Superti-Furga, G., and Brummelkamp, T. R. (2015) Gene essentiality and synthetic lethality in haploid human cells. *Science* **350,** 1092–1096 CrossRef Medline

30. Lerch-Gaggl, A., Haque, J., Li, J., Ning, G., Traktman, P., and Duncan, S. A. (2002) Pescadillo is essential for nucleolar assembly, ribosome biogenesis, and mammalian cell proliferation. *J. Biol. Chem.* **277,** 45347–45355 CrossRef Medline

31. Chen, H., Li, Z., Haruna, K., Li, Z., Li, Z., Semba, K., Araki, M., Yamamura, K., and Araki, K. (2008) Early pre-implantation lethality in mice carrying truncated mutation in the RNA polymerase 1–2 gene. *Biochem. Biophys. Res. Commun.* **365,** 636–642 CrossRef Medline

32. Newton, K., Petfalski, E., Tollervey, D., and Cáceres, J. F. (2003) Fibrillarin is essential for early development and required for accumulation of an intron-encoded small nucleolar RNA in the mouse. *Mol. Cell Biol.* **23,** 8519–8527 CrossRef Medline

33. Romanova, L. G., Anger, M., Zatsepina, O. V., and Schultz, R. M. (2006) Implication of nucleolar protein SURF6 in ribosome biogenesis and pre-implantation mouse development. *Biol. Reprod.* **75,** 690–696 CrossRef Medline

34. Hamdane, N., Stefanovsky, V. Y., Tremblay, M. G., Németh, A., Paquet, E., Lessard, F., Sanij, E., Hannan, R., and Moss, T. (2014) Conditional inactivation of upstream binding factor reveals its epigenetic functions and the existence of a somatic nucleolar precursor body. *PLoS Genet.* **10,** e1004505 CrossRef Medline

35. Zhu, Q., Yasumoto, H., and Tsai, R. Y. (2006) Nucleostemin delays cellular senescence and negatively regulates TRF1 protein stability. *Mol. Cell Biol.* **26,** 9279–9290 CrossRef Medline

36. Nicolas, E., Parisot, P., Pinto-Monteiro, C., de Walque, R., De Vleeschouwer, C., and Lafontaine, D. L. (2016) Involvement of human ribosomal proteins in nucleolar structure and p53-dependent nucleolar stress. *Nat. Commun.* **7,** 11390 CrossRef Medline

37. Brighenti, E., Treré, D., and Derenzini, M. (2015) Targeted cancer therapy with ribosome biogenesis inhibitors: a real possibility? *Oncotarget* **6,** 38617–38627 CrossRef Medline

38. Quirós, P. M., Ramsay, A. J., Sala, D., Fernández-Vizarra, E., Rodríguez, F., Peinado, J. R., Fernández-García, M. S., Vega, J. A., Enríquez, J. A., Zorzano, A., and López-Otín, C. (2012) Loss of mitochondrial protease OMA1 alters processing of the GTPase OPA1 and causes obesity and defective thermogenesis in mice. *EMBO J.* **31,** 2117–2133 CrossRef Medline

39. Fraile, J. M., Ordonez, G. R., Quiros, P. M., Astudillo, A., Galvan, J. A., Colomer, D., Lopez-Otin, C., Freije, J. M., and Puente, X. S. (2013) Identification of novel tumor suppressor proteases by degradome profiling of colorectal carcinomas. *Oncotarget* **4,** 1919–1932 CrossRef

40. Paulo, J. A., O'Connell, J. D., Gaun, A., and Gygi, S. P. (2015) Proteome-wide quantitative multiplexed profiling of protein expression: carbon-source dependency in *Saccharomyces cerevisiae*. *Mol. Biol. Cell* **26,** 4063–4074 CrossRef Medline

41. McAlister, G. C., Nusinow, D. P., Jedrychowski, M. P., Wühr, M., Huttlin, E. L., Erickson, B. K., Rad, R., Haas, W., and Gygi, S. P. (2014) MultiNotch MS3 enables accurate, sensitive, and multiplexed detection of differential expression across cancer cell line proteomes. *Anal. Chem.* **86,** 7150–7158 CrossRef Medline

42. Huttlin, E. L., Jedrychowski, M. P., Elias, J. E., Goswami, T., Rad, R., Beausoleil, S. A., Villén, J., Haas, W., Sowa, M. E., and Gygi, S. P. (2010) A tissue-specific atlas of mouse protein phosphorylation and expression. *Cell* **143,** 1174–1189 CrossRef Medline

43. Osorio, F. G., Soria-Valles, C., Santiago-Fernández, O., Bernal, T., Mittelbrunn, M., Colado, E., Rodríguez, F., Bonzon-Kulichenko, E., Vázquez, J., Porta-de la-Riva, -M., Cerón, J., Fueyo, A., Li, J., Green, A. R., Freije, J. M., and López-Otín, C. (2016) Loss of the proteostasis factor AIRAPL causes myeloid transformation by deregulating IGF-1 signaling. *Nat. Med.* **22,** 91–96 Medline

44. Subramanian, A., Tamayo, P., Mootha, V. K., Mukherjee, S., Ebert, B. L., Gillette, M. A., Paulovich, A., Pomeroy, S. L., Golub, T. R., Lander, E. S., and Mesirov, J. P. (2005) Gene set enrichment analysis: a knowledge-based approach for interpreting genome-wide expression profiles. *Proc. Natl. Acad. Sci. U.S.A.* **102,** 15545–15550 CrossRef Medline

ASBMB